A standalone, battery-free light dosimeter for ultraviolet to infrared light

David Van der Heggen Rugile Zilenaite Egle Ezerskyte Verena Fritz Katleen Korthout Dimitri Vandenberghe Johan De Grave Jan Garrevoet Laszlo Vincze Dirk Poelman Jonas J. Joos Philippe F. Smet**

Dr. David Van der Heggen, Verena Fritz, Dr. Katleen Korthout, Prof. Dirk Poelman, Dr. Jonas J. Joos, Prof. Philippe F. Smet
LumiLab, Department of Solid State Sciences, Ghent University
Krijgslaan 281/S1, 9000 Ghent, Belgium
Email Address: David.VanderHeggen@UGent.be, Philippe.Smet@UGent.be

Rugile Zilenaite, Egle Ezerskyte
Institute of Chemistry, Faculty of Chemistry and Geosciences, Vilnius University
Naugarduko Street 24, Vilnius, Lithuania

Dr. Dimitri Vandenberghe, prof. Johan De Grave
Laboratory of Mineralogy and Petrology, Department of Geology, Ghent University
Krijgslaan 281/S8, 9000 Ghent, Belgium

Dr. Jan Garrevoet
Deutsches Elektronen-Synchrotron DESY
Notkestrasse 85, Hamburg, Germany

Prof. Laszlo Vincze
XMI, Department of Chemistry, Ghent University
Krijgslaan 281/S12, 9000 Ghent, Belgium

Keywords: *luminescence, strontium aluminate, light sensor, dosimetry*

Light sensors are widely used to monitor light intensities, for instance in medical applications, in agriculture or for conservation of art. Most of these sensors are electronic devices that record continuously but applications that only require information of integrated intensities, measured over a long time, could greatly benefit from an integrating dosimeter that does not require a power supply. In this work a wireless and quantitative light dosimeter is presented based on $SrAl_2O_4$:Eu^{2+},Sm^{3+}, a phosphor that exhibits stable energy storage upon exposure to blue and ultraviolet light. It is shown that a forward electron transfer from europium to samarium can be induced under illumination with blue or ultraviolet light while the reverse electron transfer can be achieved by illuminating the phosphors with green to infrared light. This reverse transfer is accomplished through excitation of the divalent samarium and results in bright, green optically stimulated luminescence. The stable energy storage, in combination with the possibility for optical read-out, makes $SrAl_2O_4$:Eu^{2+},Sm^{3+} ideally suited to be used as an integrating light dosimeter for monochromatic to broadband light, from the ultraviolet to the near infrared. To demonstrate this, a proof of concept dosimeter was developed in which this phosphor was successfully used to measure average daylight intensities.

1 Introduction

The current state-of-the-art wireless light sensors are mostly electronic devices which continuously record light intensities over a desired wavelength range. With a few exceptions [1] these sensors have to be powered, either via near-field communication, [2] which restricts the physical operating range of the sensor, or with batteries, which limits their lifetime and makes these sensors vulnerable to water damage. Moreover, the use of batteries makes these traditional light sensors unavoidably bulky. [3,4] Printable batteries have been used to reduce the thickness of these devices but this results in increased lateral dimensions to compensate for the loss in capacity. [5] Additionally, the continuous collection of data introduces the need for data

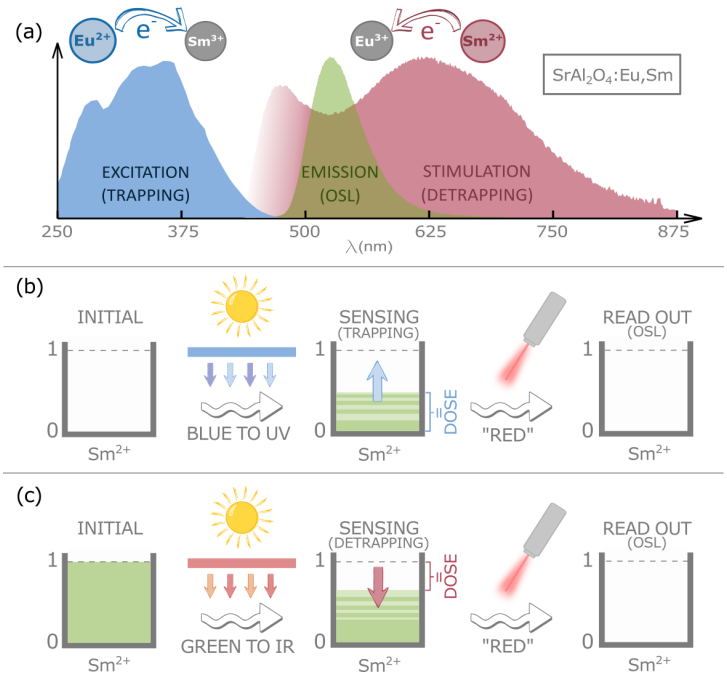

Figure 1: (a) The photoluminescence excitation (λ_{em} = 520 nm, blue curve) and emission (λ_{ex} = 445 nm, green curve) spectrum of $SrAl_2O_4$:Eu^{2+},Sm^{3+} together with the absorption spectrum of the filled traps (red curve). Schematic representation of the use of $SrAl_2O_4$:Eu^{2+},Sm^{3+} for sensing UV to blue light (b) or green to IR light (c).

logging or data transmission which requires that these sensors are equiped with memory storage or that they are located in close proximity to a receiver. [6]

Some applications only require information on the integrated light intensities, in which case many of the above-mentioned limitations can be overcome by making use of a standalone, unpowered light sensor. This is for example the case in logistics where it is necessary to quantify the integrated light exposure of light-sensitive products such as beer or other foods or pharmaceuticals, [7] in museums where monitoring of environmental factors, such as light, is of utmost importance for the preservation of art, or in precision agriculture where new techniques such as intercropping or agroforestry require an uninterupted monitoring of light intensities but where electronic devices have trouble to account for quick variations in lighting conditions. [8,9]

Such unpowered devices exist and are often based on photochromic materials which offer direct visual feedback of the dose to which the material was exposed under the form of a discoloration. However, in some cases these sensors require expensive equipment such as spectrophotometers to quantify the induced color changes, especially at low doses or when high accuracy is required. [10] Moreover, many of these sensors are based on a non-reversible discolouration of a light-sensitive material and are hence not reusable. [10,11] Herein we propose to use luminescent materials or phosphors to develop an unpowered, quantitative, reusable and low-cost integrating light sensor. Phosphors are encountered in numerous applications such as solid state lighting and displays, [12,13] thermometry, [14] scintillators [15] and solar concentrators. [16] They can be further functionalized through the addition of a suitable codopant [17] to enable energy storage upon exposure to light with a high photon energy. [18,19] In persistent phosphors this energy storage is metastable, resulting in the characteristic delayed emission or afterglow which can last from minutes up to hours after excitation has ended. This property is exploited in applications such as glow-in-the-dark watch dials, non-electrical safety signage, luminescent road markings, [20,21] visualization of stress distributions inside composites [22] or radiation-free *in vivo* medical imaging. [23,24] The best-known persistent phosphor is the green-emitting $SrAl_2O_4$:Eu^{2+},Dy^{3+} [25–27] which shows a long and intense green afterglow at room temperature thanks to the ideal depth of the involved traps. [28] Changing the codopant from dysprosium to samarium creates deeper, thermally stable trapping defects which cannot be emptied spontaneously at room temperature. [29–31]

As shown in **Figure 1(a)** trapping in $SrAl_2O_4$:Eu^{2+},Sm^{3+} can be induced using ultraviolet (UV) or blue light. Although these trapped charges are thermally stable they can be released if additional energy, under the form of green to infrared (IR) stimulation light, is provided to the trapped charges.[32–34] This in turn results in the emission of green optically stimulated luminescence (OSL) with an intensity proportional to the amount of filled traps. When combined with a suitable optical filter stack, this material can be used as an UV to IR light dosimeter of which the operational concept is illustrated in Figure 1(b,c) and explained below.

If a phosphor with maximally emptied traps is combined with an optical filter that transmits only excitation light, the sensor is configured to measure UV or blue light. Upon exposure to this excitation light the traps are gradually filled and upon read-out the OSL intensity will be directly proportional to the dose of UV and blue light to which the phosphor was exposed. If on the other hand a phosphor of which the traps are maximally filled, is combined with an optical filter that transmits only stimulation light, the sensor can also be used for longer wavelengths with a spectral sensitivity that can be tuned from green to IR. Exposure to this stimulation light will then induce a gradual depletion of the phosphor and information on the integrated dose can in this case be obtained by comparing the intensity of the residual OSL signal to the maximally obtainable intensity of a fully saturated phosphor layer. This second operational mode allows to use this material for light sensing applications at considerably longer wavelengths than what is currently achieved in, for example, phosphor-based dosimeters for ionizing radiation.[35,36] In this work we will show that it is possible to use this concept to create a unpowered, reusable light sensor that allows to quantitatively determine integrated light intensities. The design of the sensor allows to tune the spectral sensitivity and the dynamic range to meet the requirements of the envisioned application.

2 Results and Discussion

$SrAl_2O_4$:Eu^{2+},Sm^{3+} was synthesized using a conventional solid state synthesis. Both dopant concentrations and the amount of flux agent were optimized to maximize the storage capacity of the phosphor.[26] A maximal capacity was achieved for the phosphor prepared with a dopant concentration of 1 mol% of Eu and Sm with respect to Sr and 5 w% of H_3BO_3 as a flux. The relative concentration of Eu:Sm was confirmed to be 1:1 by X-ray fluorescence (XRF) measurements and the phase purity of the resulting powder was checked using powder X-ray diffraction, confirming that the powder is single phase monoclinic $SrAl_2O_4$ (JCPDS 74-0794).

The luminescence spectrum at room temperature consists of a single green emission band centered around 520 nm (Figure 1) which can be assigned to the lowest $4f^65d^1 \rightarrow 4f^7$ transition of Eu^{2+} on a Sr2 site.[37–39] In line with the expectations, no emission related to the samarium codopant is observed upon excitation at 450 nm.

In **Figure 2**(a) the afterglow and OSL intensities of $SrAl_2O_4$:Eu^{2+},Sm^{3+} are compared to the benchmark persistent phosphor $SrAl_2O_4$:Eu^{2+},Dy^{3+} and to the non-codoped material. It is clear that the singly-doped $SrAl_2O_4$:Eu^{2+} already shows fairly efficient afterglow which is greatly enhanced through the addition of the dysprosium codopant. The afterglow of $SrAl_2O_4$:Eu^{2+},Sm^{3+} on the other hand, is one and two orders of magnitude less intense compared to the non- or Dy-codoped alternatives, respectively.

Illuminating the charged phosphor with red or infrared light provides additional energy to the trapped charges, emptying the filled traps and resulting in green OSL.[40,41] It is clear that the Sm-codoped phosphor exhibits enhanced OSL intensities when compared to the Dy-codoped counterpart, indicating that the lack of room temperature afterglow in $SrAl_2O_4$:Eu^{2+},Sm^{3+} is a consequence of the enhanced thermal stability of the trapped charges and is not due to a lack of charge trapping as suggested by Aitasalo *et al.*[42] in $CaAl_2O_4$:Eu^{2+},Sm^{3+}or by Hölsä *et al.*[43] for $SrAl_2O_4$:Eu^{2+},Sm^{3+}. This is confirmed by thermoluminescence (TL) measurements shown in Figure 2(b). It can be seen that the Dy^{3+}-codoped phosphor exhibits a broad TL curve at low temperatures, which is responsible for the phosphor's excellent afterglow properties around room temperature whereas the Sm^{3+}-codoped TL curve consists mainly of a broad band above 300°C. The thermal stability of these deep traps will be discussed in detail below. Qualitative differences in shape of the afterglow and OSL curves (Figure 2) can be understood by considering that the afterglow

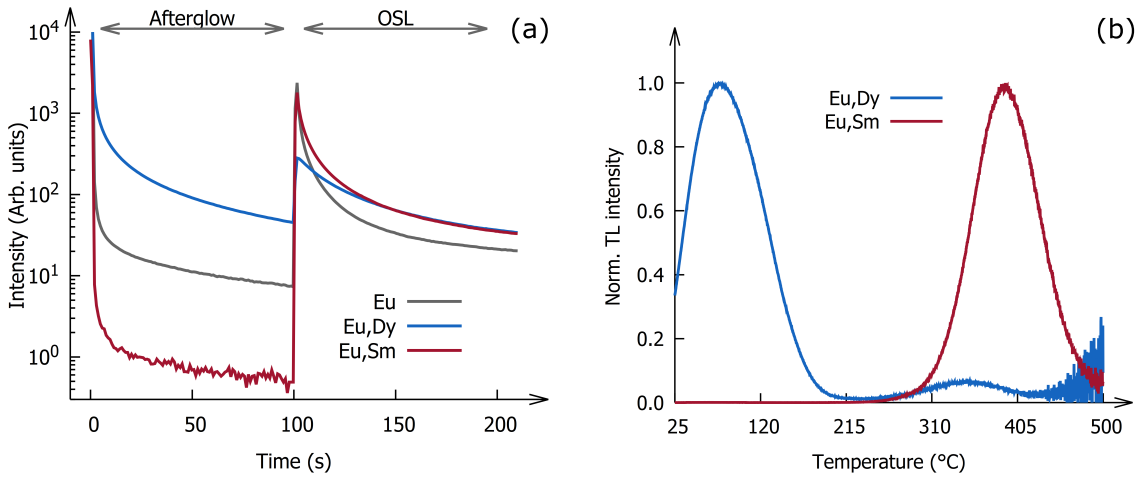

Figure 2: (a) Comparison of the afterglow and OSL response of $SrAl_2O_4$:Eu^{2+} without codoping and codoped with Dy^{3+} and Sm^{3+}. The phosphors were excited using a violet laser (λ = 405 nm). Excitation ended at t = 0 s and the infrared laser (λ = 808 nm) was switched on at t = 100 s. (b) TL curves of $SrAl_2O_4$:Eu^{2+} codoped with Dy^{3+} and Sm^{3+}, corrected for thermal quenching. TL curves were recorded at a heating rate of 0.2°C s^{-1} after excitation at 25 °C with blue light (λ = 470 nm) for 30 seconds.

originates from thermal stimulation of shallow trapping defects whereas the OSL is the result of optical stimulation of all the traps that absorb the stimulation light.

While the role of the activator ion in the persistent luminescence mechanism of strontium aluminates has already been uncovered,[44] a consensus on the chemical nature of the trapping defects has not yet been reached.[45] Recently, Joos *et al.*[46] performed X-ray spectroscopy measurements on the blue-emitting $Sr_4Al_{14}O_{25}$:Eu,Dy and they successfully identified the Dy codopant as the electron trap responsible for the afterglow in this material. This finding agrees well with the often proposed microscopic models[47] claiming that the (de-)trapping mechanism in these materials is based on the oxidation and simultaneous reduction of the activator and codopant. In the case of $SrAl_2O_4$:Eu^{2+},Sm^{3+}, this would lead to the following mechanism:

$$Eu^{2+} + Sm^{3+} \xrightarrow[BLUE]{UV} Eu^{3+} + Sm^{2+}. \quad (1)$$

$$Eu^{2+} + Sm^{3+} \xleftarrow[IR]{RED} Eu^{3+} + Sm^{2+}. \quad (2)$$

It is worth noting that the initial and final states of this charge transfer are well known but that there is still no consensus on how this transfer is accomplished,[47–49,51] however it was recently shown that the electron transfer between Eu and Sm in CaF_2 is achieved directly without the involvement of conduction band states.[50,52] To verify the existence of similar valence changes in $SrAl_2O_4$:Eu^{2+},Sm^{3+}, as suggested by Equation 1 and 2 the phosphor was subjected to a similar X-ray absorption spectroscopy experiment as described in Joos *et al.*[46] Eu L_3 and Sm L_3 X-ray absorption near edge structure (XANES) measurements performed on $SrAl_2O_4$:Eu^{2+},Sm^{3+} are shown in **Figure 3**. These data prove the coexistence of both divalent and trivalent europium and samarium. However, to link the valence changes of the dopants to the trapping process, the phosphor was alternately illuminated with UV and IR light to respectively enhance or attenuate the trapping. Figure 3(a,c) shows the XANES spectra under both illumination conditions and the difference between UV and IR illuminated samples is shown in Figure 3(b,d). From these results it is evident that excitation of the phosphor indeed induces a forward electron transfer between the dopants as described by Equation 1, whereas IR light can be used to induce the reverse electron transfer described by Equation 2. Moreover the fitting results imply that the amplitude of the change is nearly identical for europium and samarium. Since XRF confirmed a 1:1 ratio for both dopants this indicates that the trapping is largely concentrated on the samarium codopant.

The optical characteristics of the resulting divalent samarium were analyzed using diffuse reflectance measurements. By comparing the diffuse reflectance spectra of the phosphor with the traps maximally

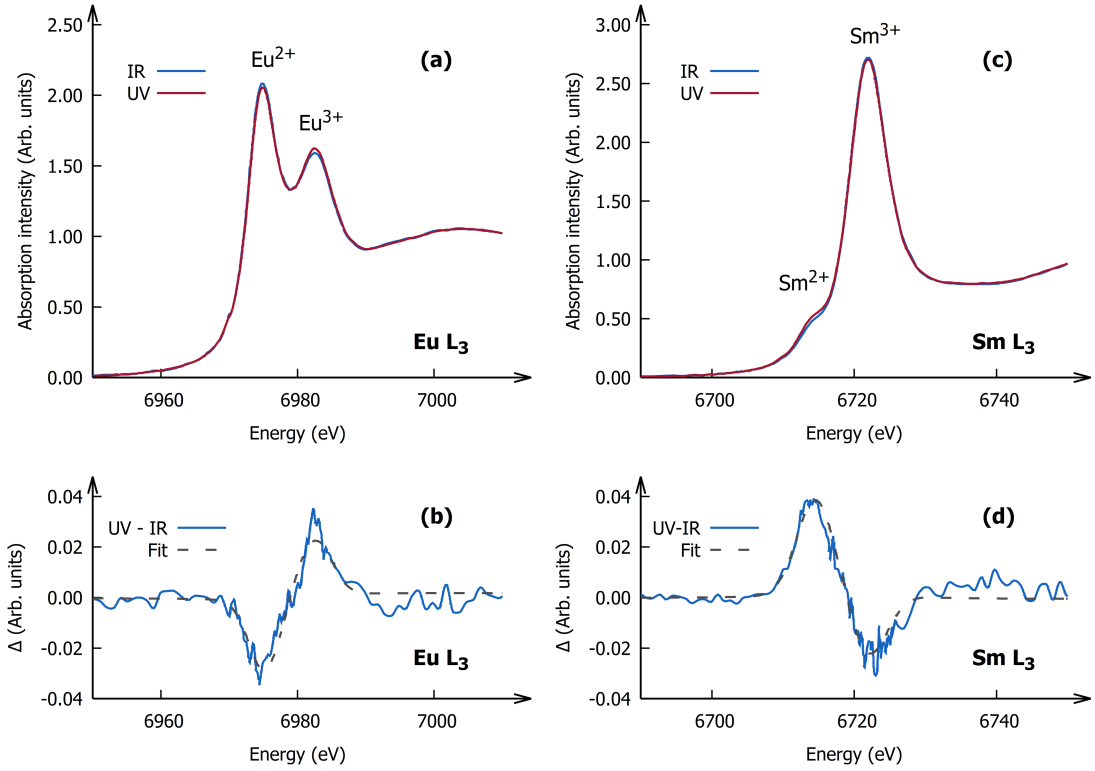

Figure 3: (a) Eu L_3 and (c) Sm L_3 XANES spectra under continuous illumination with UV and IR lasers. (b,d) The difference (UV-IR) between the XANES spectra shown in the top panels illustrating the effect of illumination.

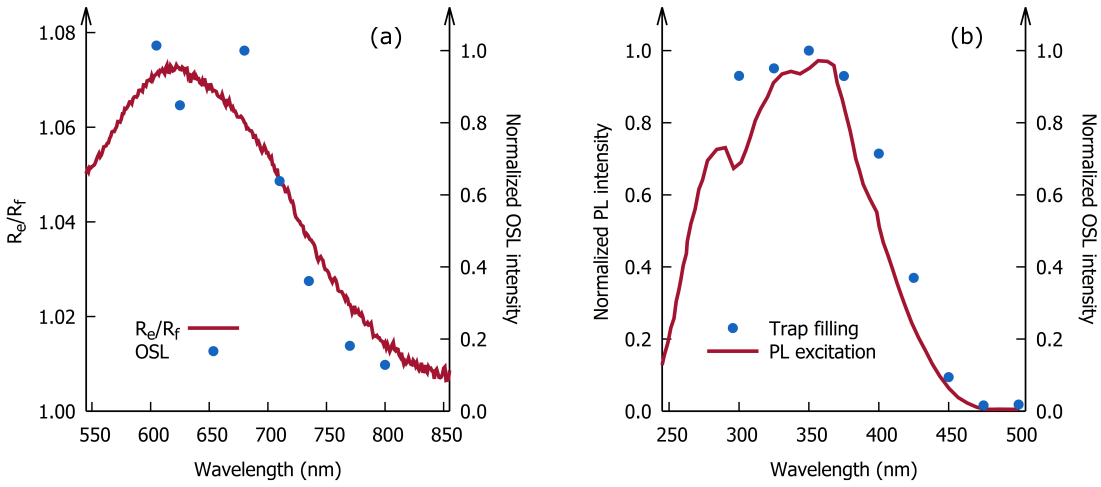

Figure 4: (a) Absorptance of the filled traps in $SrAl_2O_4$:Eu^{2+},Sm^{3+}, shown in red. The blue dots represent the dependency of the OSL intensity of $SrAl_2O_4$:Eu^{2+},Sm^{3+} on the stimulation wavelength. (b) PL excitation spectrum recorded at $\lambda_{em} = 520$ nm, shown in red. The trap filling spectrum of $SrAl_2O_4$:Eu^{2+},Sm^{3+} corresponding to the wavelength response of the sensor is shown in blue.

emptied or filled, by respectively exposing the phosphor to a blue LED or an IR lamp during 15 minutes, the absorptance spectrum of the filled traps can be determined. The ratio of the two spectra is shown in **Figure 4**(a) and consists of a broad band centered around 600 nm. At lower wavelengths the spectrum is affected by Eu^{2+} absorption, distorting the signal due to filled traps. Absorption spectra of Sm^{2+} in halide and fluoride crystals have been extensively studied and are found at slightly higher energies than the absorption band recorded here.[53] However, considering the well documented redshift of the $4f^n \rightarrow 4f^{n-1}5d^1$ transition energies of divalent lanthanides when going from a fluoride to an oxide host,[54] it can be concluded that this absorption band can be attributed to Sm^{2+}.

An OSL excitation spectrum was recorded by exposing the fully charged phosphor to light with different wavelengths and integrating the OSL emitted during the first 5 minutes of stimulation. The result is overlaid on the absorptance spectrum of the Sm^{2+} in Figure 4(b) from which it is evident that the stimulation efficiency exhibits the same wavelength dependency as the absorptance. From this it can be concluded that the reverse electron transfer described in Equation 2 can be induced through direct excitation of Sm^{2+}. Similarly, a trap filling spectrum was recorded, by exposing the uncharged phosphor to excitation light with a varying wavelength and subsequently recording the OSL intensity, immediately after illumination with excitation light stopped. This trap filling spectrum represents the wavelength response curve of a sensor based on this material and is shown in Figure 4(b), superimposed on the PL excitation spectrum. From the similarity between the two it can be deduced that excitation of the Eu^{2+} activator is required to induce trapping in $SrAl_2O_4$:Eu^{2+},Sm^{3+}. This is in line with persistent luminescence excitation spectra recorded on $SrAl_2O_4$:Eu^{2+},Dy^{3+}.[55]

The combination of stable energy storage upon exposure to UV and blue light and the possibility for optical read-out makes it possible to use this phosphor as an optical dosimeter. This requires a detailed evaluation of the phosphor's dose response and fading characteristics.[56] A dose dependency measurement was carried out by exposing the phosphor to different amounts of blue light with a wavelength of 450 nm and integrating the resulting OSL output under stimulation with red light (λ = 660 nm). The results are shown in **Figure 5**(a) from which it is clear that the OSL output is initially linearly dependent on the applied dose up to an integrated dose of 19.5 mJ cm^{-2}. This is equivalent to an exposure of a few seconds to direct sunlight but, as shown by the proof of concept measurement discussed below, the dynamic range of the sensor can easily be extended to higher integrated doses by making use of neutral density filters. This value of 19.5 mJ cm^{-2} will be different for other phosphor compositions and depends on the storage capacity of the phosphor, the absorption strength for the wavelengths to be measured and the trapping probability following this absorption. At higher doses the OSL intensity saturates implying a maximum filling of the traps is achieved.

The stability of the signal over time was tested in a conventional fading experiment during which the phosphor is charged into saturation and the time between the end of charging and optical stimulation is varied from 1 to 1120 minutes. It is evident from Figure 5(b) that the signal fades quickly during the first two hours, after which the remaining signal stabilizes at around 60% of the original intensity. This fading is an undesired effect for dosimetric applications but as the TL fading experiment in Figure 5(c) shows, this is due to the presence of unwanted shallow trapping defects which are also responsible for the material's limited afterglow shown in Figure 2(a). In contrast, the deep, samarium-related traps which are of interest for the dosimetric application proposed in this work, give rise to the glow peak centred around 400°C (Figure 2(b)) and are stable at room temperature. Upon stimulation with red light, both shallow and deep traps are emptied which explains why the OSL signal in Figure 5(b) initially fades. These unwanted shallow traps are not related to the samarium codopant but could presumably stem from trace amounts of impurities or intrisic defects. An electron paramagnetic spectroscopy study on $SrAl_2O_4$:Eu^{2+} has already indicated that low concentrations of transition metal ions are often unintentionally incorporated in persistent phosphors, influencing the afterglow properties of the final material.[57] However, a preliminary optimization study has shown that an electron-beam annealing treatment in vacuum can be used to largely suppress this fading, with a signal loss of only 22% after one day of storage.[58]

In addition to a preferably linear dose response and minimal fading, the response of a dosimeter should be independent of the dose rate. Put differently, the OSL intensity should be the same for an identical

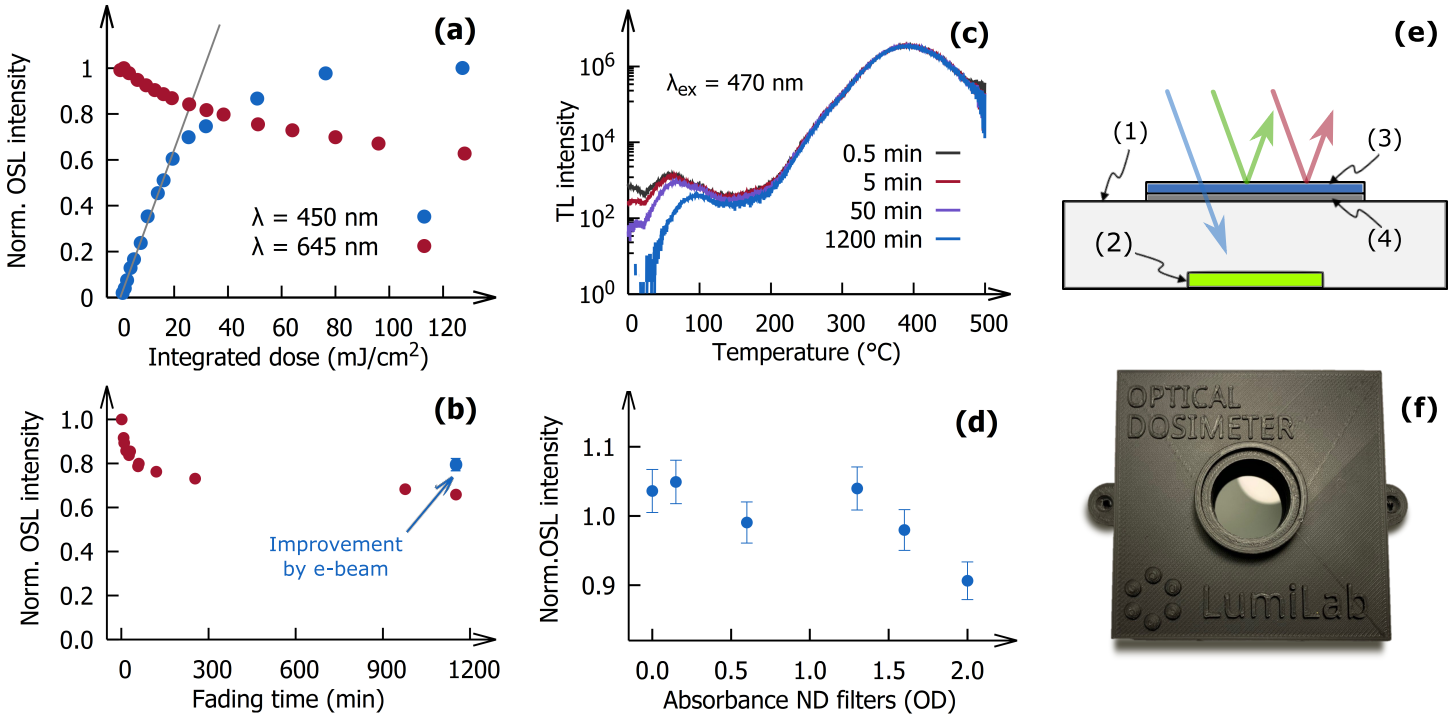

Figure 5: (a) Dose dependency of the OSL intensity after illuminating an empty phosphor with different doses of blue light or after illuminating a saturated phosphor with different amounts of red light (645 nm, 0.64 mW cm^{-2}) (b) Fading characteristics showing the decrease in OSL intensity when the time between excitation with blue light and OSL is varied. The effect of the electron-beam annealing treatment is shown in blue. (c) Thermoluminescence fading experiment. The curves were recorded after illuminating the phosphor with blue (λ = 470 nm) light and waiting for the specified amount of time. (d) Effect of the dose rate on the OSL intensity. (e) A schematic overview of the light dosimeter comprising a light-tight casing (1), a polymer layer containing $SrAl_2O_4$:Eu^{2+},Sm^{3+} (2), a shortpass or bandpass filter (3) and a neutral density filter (4). (f) The proof of concept light sensor used for the measurement of the daylight intensities.

number of incident UV or blue photons: a short exposure to light with a high intensity should give the same result as a long exposure to light with a low intensity. This was tested using neutral density filters with different optical densities (OD) to expose the phosphor to light with different intensities. For each filter the illumination time is varied, going from 5 seconds (OD = 0) to 500 seconds (OD = 2), to ensure the integrated dose is equal to 19.5 mJ/cm^{-2} for all illumination intensities. The results are shown in Figure 5(d) and it is clear that the OSL intensity deviates slightly with a decrease of only 10% when the excitation intensity is varied over two orders of magnitude. This shows that the optical response of the material is indeed independent of the applied dose rate. A further lowering of the dose rate should therefore not present any problems, provided that the integrated dose still results in an OSL signal that is bright enough to be detected during readout. The slight decrease in OSL intensity at lower excitation intensities, and therefore longer excitation times, is related to the fading shown in Figure 5(b).

While the measurements above were performed with a 450 nm LED as the excitation source, the trap filling spectrum in Figure 4(b) shows that similar results can be obtained for all wavelengths between 250 nm and 475 nm. However, as illustrated in Figure 1 the material can also be configured to measure intensities of light with a longer wavelength, provided that this light can induce optically stimulated detrapping. The phosphor is first exposed to UV or blue light prior to the measurement to ensure maximal trap filling. Exposure of this saturated phosphor layer to the longer wavelength light will then lead to a gradual depletion of the phosphor. Figure 5(a) shows the dependency of the OSL signal of a fully saturated phosphor layer after exposure to different amounts of red light (λ = 645 nm). The effect of fading was taken into account by keeping the time between excitation with blue light and read-out fixed, independent of the illumination time. The decrease of the OSL signal in Figure 5(a) is therefore only due to exposure of the phosphor to red light, illustrating that the material can indeed be used to measure intensities of light with a wavelength between 500 nm and 850 nm as well (see Figure 4(a)).

To demonstrate the potential of $SrAl_2O_4$:Eu^{2+},Sm^{3+} in real light sensing applications, a proof of concept light dosimeter (Figure 5(e)) was developed consisting of a lightproof box (1) containing a phosphor loaded polymer disk (2). The top of the box contained two filters: a 450 nm shortpass filter (3) and a neutral density filter (4). The former prevents exposure of the sample to red or infrared light which, as shown in Figure 4(b), induces optical detrapping. The latter is used to increase the dynamic range of the demonstrator, which is primarily determined by the saturation behaviour shown in Figure 5(a), towards higher intensities. A proof of concept light dosimeter (Figure 5(f)) and a conventional, continuously recording, electronic lux-meter (TSL 2561) were used side-by-side to measure average daylight intensities during four consecutive days. To ensure that the traps were maximally emptied before exposing the dosimeter to ambient light during the measurement, the light sensitive layer containing $SrAl_2O_4$:Eu^{2+},Sm^{3+} was exposed to red stimulation light (laser, 660 nm, 70 mW) prior to every measurement in order to let the OSL signal of a charged or saturated phosphor drop to the background level. Approximately 1.5 hours after sunset, the dosimeter was 'read out' by exposing the phosphor loaded polymer layer to the stimulation light and recording the OSL intensity. The result of these measurements are shown in **Figure 6**(a-d). The blue curves represent the time-resolved daylight intensity as measured by the electronic lux-meter. The large variations in daylight intensity are a consequence of the varying weather conditions. The corresponding average intensities recorded by the electronic lux-meter and the dosimeter are represented by the blue and red bars, respectively. It can be seen from Figure 6(e) that a good agreement is achieved between the values obtained by the two sensors and that the values deviate at most 10% with the reference measurements while the integrated daylight intensities vary over one order of magnitude. It should be kept in mind that the fraction of blue and UV light in daylight varies throughout the day and is also dependent on the weather conditions. Comparing the results of the proof of concept sensor (which only records blue and UV light intensities) to the results of the electronic lux-meter (sensitive for all visible wavelengths) will therefore inevitably introduce some small uncertainty.

Overall, this shows that luminescent materials such as $SrAl_2O_4$:Eu^{2+},Sm^{3+} can effectively be used to develop an integrating light sensor. Moreover this light dosimeter is completely standalone and does not require external power sources or memory storage, thereby offering a large advantage over conventional powered light sensors. The dynamic and spectral range can easily be tuned by combining several dosimeters

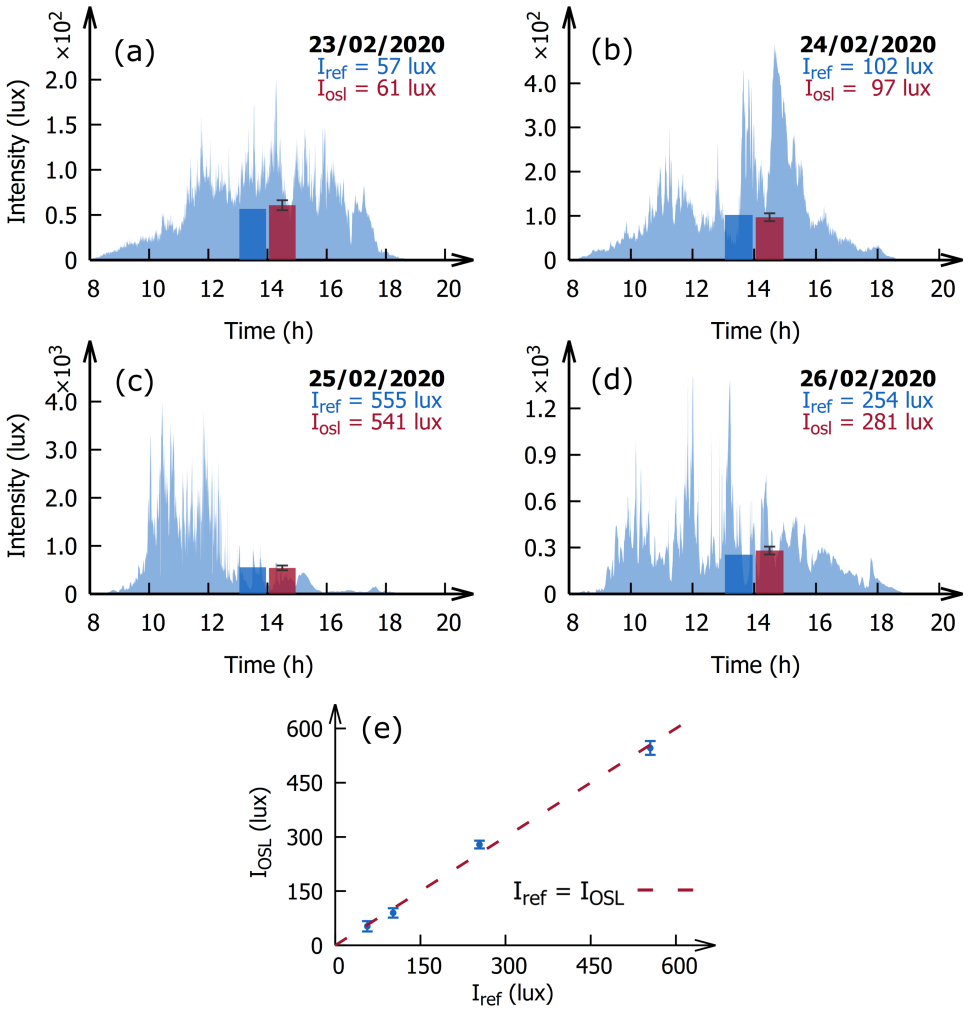

Figure 6: (a-d) Measurements of the daylight intensity in Ghent (Belgium) during four consecutive days. The blue graph indicates the time-resolved daylight intensity as measured with an electronic lux-meter and the blue bar indicates the corresponding average daylight intensity. The red bar represents the average intensity as recorded with the proof of concept light dosimeter. (e) Comparison of the daylight intensities measured using the two techniques.

with different neutral density or color filters. Moreover one can easily think of using the concept outlined in this section to include other applications such as a UV index sensor, which only requires a different short-pass filter to be used.

3 Conclusion

The luminescence and energy storage properties of $SrAl_2O_4$:Eu^{2+},Sm^{3+} were investigated. X-ray spectroscopy and diffuse reflectance measurements, both in combination with illumination with blue and (infra)red light, have confirmed that the samarium codopant directly participates in the trapping process and acts as an electron trap. An OSL excitation spectrum was measured and it was found that it coincides with the absorption bands of Sm^{2+}. Correspondingly, it can be concluded that excitation of the Sm^{2+} ions, which are formed during the trapping process, induces an electron back transfer and results in optically stimulated luminescence. To evaluate the applicability of $SrAl_2O_4$:Eu^{2+},Sm^{3+} in dosimetric applications, the dose dependency as well as the fading characteristics of $SrAl_2O_4$:Eu^{2+},Sm^{3+} have been investigated. These measurements showed that some fading occurs during the first two hours after illumination but that the signal essentially stabilises at around 60% of the original intensity. However, an electron-beam annealing treatment has allowed to reduce this fading to 78%. Further tweaking of the annealing procedure might offer a way to fully eliminate this undesired effect. Finally, a proof of concept light dosimeter was built to demonstrate that $SrAl_2O_4$:Eu^{2+},Sm^{3+} can be used as a sensor to measure average daylight intensities. Comparison with a conventional electronic lux-meter shows that $SrAl_2O_4$:Eu^{2+},Sm^{3+} is perfectly suited for light sensing applications from the UV to the IR, offering the additionally advantage of being completely standalone and relatively low-cost.

4 Experimental Section

Synthesis

$SrAl_2O_4$:Eu^{2+} and $SrAl_2O_4$:Eu^{2+},Sm^{3+} were synthesized by mixing stoichiometric amounts of Al_2O_3, Sm_2O_3, Eu_2O_3 and $SrCO_3$ (Alfa Aesar, 99.99%) and subsequently heating the mixture to 1450°C in a reducing atmosphere (10% of H_2 in N_2) during 4 hours. Boric acid (H_3BO_3, >99.8%, Honeywell) was added as a flux agent. Optically stimulated luminescence measurements were performed on a phosphor loaded polymer layer. To this end the phosphor was mixed with an appropriate amount of Sylgard-184 elastomer (8:1 mass ratio, base to curing agent) and heated to 50°C for 1 hour. The $SrAl_2O_4$:Eu^{2+},Dy^{3+} was commercial phosphor, acquired from GloTech International Ltd.

E-beam annealing was performed in a Leybold Univex 450 vacuum system equipped with an e-beam evaporation source (8kV, max. 400mA) according to the procedure outlined in Smet *et al.*[58]

Structural and optical characterization

Powder X-ray diffraction (XRD) analysis was conducted with a Siemens D5000 diffractometer using Cu Kα radiation. Photoluminescence excitation and emission spectra were recorded with a Edinburgh Instruments FS920 fluorescence spectrometer. Diffuse reflectance spectra were obtained using a Perkin Elmer Lambda 1050 UV-VIS-NIR multifunctional spectrophotometer equipped with an integrating sphere.

The OSL was recorded with a fiber-coupled, cooled QE65000 spectrometer (Ocean Optics). Unless otherwise stated, excitation of the phosphor was achieved using a 5 mm blue light emitting diode (LED) (450 nm, 42.3 μW cm^{-2}) and stimulation of the phosphor was performed using a red diode laser (660 nm, 70 mW). Appropriate shortpass filters ($\lambda_{cut-off}$= 500 or 650 nm) were used to discriminate between stimulation light and emission from the phosphor.

The OSL excitation spectrum was recorded using a set of 5 mm LEDs (λ = 605, 625, 680, 710, 735, 770 and 800 nm). An intensity calibration was performed using a LS-1-CAL halogen lamp (Ocean Optics) to ensure a constant photon flux during stimulation, independent of the simulation wavelength.

The trap filling spectrum was recorded using the monochromated xenon arc lamp from the Edinburgh Instruments FS920 fluorescence spectrometer as an excitation source. The intensity of the excitation light was measured with a S401C thermal power sensor coupled to a PM400 read-out console (Thorlabs Inc.) and the spectrum was corrected for differences in excitation intensity.

The TL measurements were performed using an automated Risø TL/OSL reader equipped with blue (λ_{max} = 470 nm, FWHM = 32 nm) LEDs providing an excitation intensity of 0.55 mW cm^{-2} at sample position. All glow curves were recorded while heating under a nitrogen atmosphere. A combination of a Schott BG39 and a Schott BG3 filter was used in front of the PMT, enabling detection of the green TL signal. Excitation of the phosphor was always carried out at room temperature, using blue light.

An electronic TSL 2561 lux meter was used as a reference for the proof of concept measurements.

X-ray absorption spectroscopy

XANES measurements were performed at the L_3 edge of the rare earth dopants and recorded in fluorescence mode at the DUBBLE (Dutch-Belgian beamline, BM26A) and the SNBL (Swiss-Norwegian beamline, BM01) beamlines of the 6 GeV ESRF (European Synchrotron Radiation Facility) in Grenoble, France. The synchrotron radiation was monochromated with a double Si(111) monochromator in conjunction with higher harmonic suppression. At the DUBBLE beamline the fluorescence emission was detected using a 9-element monolithic Ge detector, while at the SNBL beamline a 13-element Ge detector was used. The fitting procedure for the quantitative analysis of XANES spectra is analogous as the procedure described in Joos *et al.* [46,52] and consisted of a least squares fitting of the difference between the experimental data and the simulated spectra. The spectra were fitted using a Gaussian function to describe the white lines whereas the the step-like function, caused by the transition of the $2p_{3/2}$ electron to the continuum or quasi continuum states was described by an arctangent.

X-ray Fluorescence

The XRF measurements were performed using a monochromatic excitation based micro-XRF spectrometer tuned specifically for high-sensitivity quantitative elemental analysis. [59] The excitation energy was 17.4 keV, generated by a commercially available Mo-target microfocus X-ray source equipped with a Doubly Curved Crystal (DCC) optics (X-ray Optical Systems, Albany, NY, USA). The XRF radiation was detected under 90° relative to the incoming X-ray beam by a SiriusSD Silicon Drift detector (e2v, Essex, United Kingdom), having an active area of 60 mm^2.

Acknowledgements

D.V.d.H. acknowledges the financial support from the Industrial Research Fund (IOF) of Ghent university (F2020/IOF-ConpTT/094). J.J.J. is grateful to the UGent Special Research Fund (BOF) for financial support (BOF/PDO/2017/002101). P.F.S. acknowledges the UGent Special Research Fund (BOF) for funding through the GOA project "ENCLOSE". J.G. was supported by a Ph.D. grant of the Agency for Innovation by Science and Technology (IWT). The authors acknowledge the financial support from the FWO (project I002418N).

References

[1] S. Y. Heo, J. Kim, P. Gutruf, A. Banks, P. Wei, R. Pielak, G. Balooch, Y. Shi, H. Araki, D. Rollo, C. Gaede, M. Patel, J. Won Kwak, A. E. Peña-Alcántara, K.-T. Lee, Y. Yun, J. K. Robinson, S. Xu, J. A. Rogers, *Sci. Transl. Med.* **2018**, *10* eaau1643.

[2] J. Kim, G. A. Salvatore, H. Araki, A. M. Chiarelli, Z. Xie, A. Banks, X. Sheng, Y. Liu, J. W. Lee, K. I. Jang, S. Y. Heo, K. Cho, H. Luo, B. Zimmerman, J. Kim, L. Yan, X. Feng, S. Xu, M. Fabiani, G. Gratton, Y. Huang, U. Paik, J. A. Rogers, *Sci. Adv.* **2016**, *2*, 8 e1600418.

[3] A. J. Bandodkar, I. Jeerapan, J. Wang, *ACS Sens.* **2016**, *1*, 5 464.

[4] G. Xu, C. Cheng, Z. Liu, W. Yuan, X. Wu, Y. Lu, S. S. Low, J. Liu, L. Zhu, D. Ji, S. Li, Z. Chen, L. Wang, Q. Yang, Z. Cui, Q. Liu, *Adv. Mater. Technol.* **2019**, *4*, 7 1800658.

[5] W. H. Cheong, B. Oh, S. H. Kim, J. Jang, S. Ji, S. Lee, J. Cheon, S. Yoo, S. Y. Lee, J. U. Park, *Nano Energy* **2019**, *62* 230.

[6] H. Araki, J. Kim, S. Zhang, A. Banks, K. E. Crawford, X. Sheng, P. Gutruf, Y. Shi, R. M. Pielak, J. A. Rogers, *Adv. Fun. Mater.* **2017**, *27*, 2 1604465.

[7] I. Caballero, C. A. Blanco, M. Porras, *Trends Food Sci. Technol.* **2012**, *26*, 1 21.

[8] A. Rosati, K. J. Wolz, L. Murphy, L. Ponti, S. Jose, *Agric. For. Meteorol.* **2020**, *284* 107892.

[9] U. Shafi, R. Mumtaz, J. García-Nieto, S. A. Hassan, S. A. R. Zaidi, N. Iqbal, *Sensors* **2019**, *19*, 17 3796.

[10] W. Zou, M. Sastry, J. J. Gooding, R. Ramanathan, V. Bansal, *Adv. Mater. Technol.* **2020**, *5*, 4 1901036.

[11] W. Kurz, A. K. Yetisen, M. V. Kaito, M. J. Fuchter, M. Jakobi, M. Elsner, A. W. Koch, W. Kurz, A. K. Yetisen, M. V. Kaito, M. Jakobi, A. W. Koch, M. J. Fuchter, M. Elsner, *Adv. Opt. Mater.* **2020**, *8* 1901969.

[12] Z. Xia, A. Meijerink, *Chem. Soc. Rev.* **2017**, *46*, 1 275.

[13] P. Pust, V. Weiler, C. Hecht, A. Tücks, A. S. Wochnik, A. K. Henß, D. Wiechert, C. Scheu, P. J. Schmidt, W. Schnick, *Nat. Mater.* **2014**, *13*, 9 891.

[14] M. Quintanilla, L. M. Liz-Marzán, *Nano Today* **2018**, *19* 126.

[15] S. Liu, J. A. Mares, X. Feng, A. Vedda, M. Fasoli, Y. Shi, H. Kou, A. Beitlerova, L. Wu, C. D'Ambrosio, Y. Pan, M. Nikl, *Adv. Opt. Mater.* **2016**, *4*, 5 731.

[16] J. Roncali, *Adv. Energy Mater.* **2020**, *10*, 36 2001907.

[17] J. J. Joos, D. Van der Heggen, L. I. D. J. Martin, L. Amidani, P. F. Smet, Z. Barandiarán, L. Seijo, *Nat. Commun.* **2020**, *11* 3647.

[18] K. Van den Eeckhout, P. F. Smet, D. Poelman, *Materials* **2010**, *3*, 4 2536.

[19] J. Xu, S. Tanabe, *J. Lumin.* **2019**, *205* 581.

[20] D. Poelman, D. Van der Heggen, J. Du, E. Cosaert, P. F. Smet, *J. Appl. Phys.* **2020**, *128* 240903.

[21] J. Botterman, P. F. Smet, *Opt. Express* **2015**, *23*, 15 A868.

[22] C. N. Xu, X. G. Zheng, M. Akiyama, K. Nonaka, T. Watanabe, *Appl. Phys. Lett.* **1999**, *76*, 2 179.

[23] T. Maldiney, A. Bessiere, J. Seguin, E. Teston, S. K. Sharma, B. Viana, A. J. J. Bos, P. Dorenbos, M. Bessodes, D. Gourier, D. Scherman, C. Richard, *Nat. Mater.* **2014**, *13*, 4 418.

[24] J. Xu, D. Murata, J. Ueda, B. Viana, S. Tanabe, *Inorg. Chem.* **2018**, *57*, 9 5194.

[25] T. Matsuzawa, Y. Aoki, N. Takeuchi, Y. Murayama, *J. Electrochem. Soc.* **1996**, *143*, 8 2670.

[26] D. Van der Heggen, J. J. Joos, D. Rodríguez Burbano, J. Capobianco, P. F. Smet, *Materials* **2017**, *10*, 8 867.

[27] J. Bierwagen, T. Delgado, G. Jiranek, S. Yoon, N. Gartmann, B. Walfort, M. Pollnau, H. Hagemann, *J. Lumin.* **2020**, *222* 117113.

[28] J. Du, O. Q. De Clercq, D. Poelman, *Sci. Rep.* **2019**, *9* 10517.

[29] Y. Gao, R. Li, W. Zheng, X. Shang, J. Wei, M. Zhang, J. Xu, W. You, Z. Chen, X. Chen, *Chem. Sci.* **2019**, *10* 5452.

[30] P. Dorenbos, A. Bos, N. Poolton, *Opt. Mater.* **2011**, *33*, 7 1019.

[31] D. Lapraz, H. Prévost, G. Angellier, F. Mady, M. Benabdesselam, L. Dusseau, *Phys. Status Solidi A* **2007**, *204*, 12 4281.

[32] D. Van der Heggen, D. R. Cooper, M. Tesson, J. J. Joos, J. Seuntjens, J. A. Capobianco, P. F. Smet, *Nanomaterials* **2019**, *9*, 8 1127.

[33] D. C. Rodriguez Burbano, S. K. Sharma, P. Dorenbos, B. Viana, J. A. Capobianco, *Adv. Opt. Mater.* **2015**, *3*, 4 551.

[34] L. Yuan, Y. Jin, Y. Su, H. Wu, Y. Hu, S. Yang, *Laser Photonics Rev.* 2000123.

[35] C. Wang, X. Yang, J.H. Zang, Y. Chen,C. Lin, Z. Liu, C. Shen, *Chin. Phys. B* **2020**, *29*, 058504

[36] Y. Liu, Z. Chen, Y. Fan, W. Ba, W. Lu, Q. Guo, S. Pan, A. Chang, X. Tang, *Prog. Nat. Sci.* **2008**, *18*, 10 1203

[37] D. Dutczak, T. Jüstel, C. Ronda, A. Meijerink, *Phys. Chem. Chem. Phys.* **2015**, *17* 15236.

[38] L. Ning, X. Huang, Y. Huang, P. A. Tanner, *J. Mater. Chem. C* **2018**, *6* 6637.

[39] M. Nazarov, M. Brik, D. Spassky, B. Tsukerblat, *J. Lumin.* **2017**, *182* 79.

[40] E. G. Yukihara, S. W. S. McKeever, *Phys. Med. Biol.* **2008**, *53*, 20 R351.

[41] R. Chen, S. W. S. McKeever, *Theory of Thermoluminescence and Related Phenomena*, World Scientific, **1997**.

[42] T. Aitasalo, P. Dereń, J. Hölsä, H. Jungner, J.-C. Krupa, M. Lastusaari, J. Legendziewicz, J. Niittykoski, W. Stręk, *J. Solid State Chem.* **2003**, *171*, 1-2 114.

[43] J. Hölsä, H. Jungner, M. Lastusaari, J. Niittykoski, *J. Alloys Compd.* **2001**, *323-324* 326.

[44] K. Korthout, K. Van den Eeckhout, J. Botterman, S. Nikitenko, D. Poelman, P. F. Smet, *Phys. Rev. B* **2011**, *84*, 8 085140.

[45] V. Vitola, D. Millers, I. Bite, K. Smits, A. Spustaka, *Mater. Sci. Technol.* **2019**, *35*, 14 1661.

[46] J. J. Joos, K. Korthout, L. Amidani, P. Glatzel, D. Poelman, P. F. Smet, *Phys. Rev. Lett.* **2020**, *125* 033001.

[47] P. Dorenbos, *J. Electrochem. Soc.* **2005**, *152*, 7 H107.

[48] F. Clabau, X. Rocquefelte, S. Jobic, P. Deniard, M.-H. Whangbo, A. Garcia, T. Le Mercier, *Chem. Mater.* **2005**, *17*, 15 3904.

[49] G. A. Mandl, D. Van der Heggen, D. R. Cooper, J. J. Joos, J. Seuntjens, P. F. Smet, J. A. Capobianco, *Nanoscale* **2020**, *12* 20759.

[50] J. J. Joos, I. Neefjes, L. Seijo, Z. Barandiarán , *J. Chem. Phys.* **2021**, *154*, 064704.

[51] C. MacKeen, F. Bridges, L. Seijo, Z. Barandiarán, M. Kozina, A. Mehta, M. F. Reid, J. P. Wells, *J. Phys. Chem. C* **2017**, *121*, 51 28435.

[52] J. J. Joos, D. Van der Heggen, L. Amidani, L. Seijo, Z. Barandiarán *Phys. Rev. B* **2021**, *104*, L201108

[53] E. Loh, *Phys. Rev.* **1968**, *175*, 2 533.

[54] P. Dorenbos, *J. Lumin.* **2003**, *104*, 4 239.

[55] H. Liu, B. Feng, L. Luo, C. Han, P. A. Tanner, *Opt. Mater. Express* **2016**, *6*, 11 3375.

[56] P. A. Jursinic, *Med. Phys.* **2007**, *34*, 12 4594.

[57] P. Boutinaud, D. Boyer, A. Perthue, R. Mahiou, E. Cavalli, M. G. Brik, *J. Lumin.* **2015**, *159* 158.

[58] P. F. Smet, N. Avci, K. Van den Eeckhout, D. Poelman, *Opt. Mater. Express* **2012**, *2*, 10 1306.

[59] J. Garrevoet, B. Vekemans, S. Bauters, A. Demey, L. Vincze, *Anal. Chem.* **2015**, *87*, 13 6544.